Electrotonic coupling of excitable and nonexcitable cells in the heart revealed by optogenetics

T. Alexander Quinn[a,1,2], Patrizia Camelliti[b,1], Eva A. Rog-Zielinska[c,1], Urszula Siedlecka[c], Tommaso Poggioli[c], Eileen T. O'Toole[d], Thomas Knöpfel[e], and Peter Kohl[c,f,2]

[a]Department of Physiology and Biophysics, Dalhousie University, Halifax, NS B3H 4R2, Canada; [b]School of Biosciences and Medicine, University of Surrey, Guildford GU2 7XH, United Kingdom; [c]National Heart and Lung Institute, Imperial College London, Harefield UB9 6JH, United Kingdom; [d]Department of Molecular, Cellular and Developmental Biology, University of Colorado, Boulder, CO 80309; [e]Department of Medicine, Imperial College London, London W12 0NN, United Kingdom; and [f]Institute for Experimental Cardiovascular Medicine, University Heart Centre Freiburg/Bad Krozingen, Medical School of the University of Freiburg, 79110 Freiburg, Germany

Edited by Clara Franzini-Armstrong, University of Pennsylvania Medical Center, Philadelphia, PA, and approved November 11, 2016 (received for review July 8, 2016)

Electrophysiological studies of excitable organs usually focus on action potential (AP)-generating cells, whereas nonexcitable cells are generally considered as barriers to electrical conduction. Whether nonexcitable cells may modulate excitable cell function or even contribute to AP conduction via direct electrotonic coupling to AP-generating cells is unresolved in the heart: such coupling is present in vitro, but conclusive evidence in situ is lacking. We used genetically encoded voltage-sensitive fluorescent protein 2.3 (VSFP2.3) to monitor transmembrane potential in either myocytes or nonmyocytes of murine hearts. We confirm that VSFP2.3 allows measurement of cell type-specific electrical activity. We show that VSFP2.3, expressed solely in nonmyocytes, can report cardiomyocyte AP-like signals at the border of healed cryoinjuries. Using EM-based tomographic reconstruction, we further discovered tunneling nanotube connections between myocytes and nonmyocytes in cardiac scar border tissue. Our results provide direct electrophysiological evidence of heterocellular electrotonic coupling in native myocardium and identify tunneling nanotubes as a possible substrate for electrical cell coupling that may be in addition to previously discovered connexins at sites of myocyte–nonmyocyte contact in the heart. These findings call for reevaluation of cardiac nonmyocyte roles in electrical connectivity of the heterocellular heart.

cardiac | electrophysiology | fibroblast | heterocellular coupling | genetically-encoded voltage indicator

Heart muscle is composed of electrically excitable [i.e., action potential (AP)-generating] myocytes, which perform the mechanical core work essential for cardiac function, and nonexcitable (incapable of AP generation) nonmyocytes, which are crucial for cardiac development, structural integrity, biochemical signaling, and tissue repair (1). Nonmyocytes, mainly interstitial and endothelial cells, represent a heterogeneous, dynamic group of nonexcitable cells that outnumber myocytes, although they occupy a smaller volume fraction (2). Whereas paracrine and structural roles of nonmyocytes are well-established in the mammalian heart, awareness of their potential role in electrical signal propagation has only started to emerge (3, 4).

According to current concepts, the cardiac interstitium (consisting of extracellular matrix and cells) forms barriers to AP conduction—most notably in fibrous layers that separate sequentially activated heart regions or in postinjury scars. The possibility that nonmyocytes may contribute to cardiac electrical connectivity is not generally considered in situ and would require direct electrotonic connections between cardiac myocytes and nonmyocytes in native heart tissue.

Such heterocellular electronic coupling could involve connexin proteins found at points of cardiomyocyte–nonmyocyte contact in the myocardium (5). Possible functionality of connexin-based junctions was indicated in rabbit atrium, where dye diffusion between heterotypic cell types has been reported (6), and in mouse ventricle, where fibroblast-specific conditional connexin 43 knockout reduced transmission of injected current from healthy to scarred tissue (7). A number of clinical observations, such as transscar electrical conduction after atrial ablation (8) or surgical repair of congenital heart defects (9) and transplantation (10), in addition to experimental findings of electrical conduction into postinfarct (11) and cryoinjury (7) scars and along implanted tissue grafts (12, 13) would be in keeping with a (passive) contribution by nonmyocytes to cardiac AP conduction. Functional heterocellular electrotonic coupling thus far has been shown conclusively in vitro only [where it is aided by phenotype conversion and connexin overexpression of cultured fibroblasts (14–17)]. Direct confirmation in situ by classic electrophysiological means is lacking, perhaps because the high membrane resistance and low capacitance of fibroblasts mean that myocytes "AP-clamp" directly coupled fibroblasts (18). As a result, microelectrode recordings cannot reliably distinguish electrotonically coupled nonmyocytes from myocytes in native heart tissue. Surface electrical and dye-based optical mapping of multicellular activity equally cannot assess heterocellular coupling, because these signals are not population-specific and are dominated by cardiomyocyte activity.

In contrast, optogenetic techniques allow for cell type-specific recordings. To determine whether heterocellular electrotonic coupling occurs in native myocardium, we expressed an mCerulean-Citrine (CFP-YFP) FRET-based voltage reporter [voltage-sensitive fluorescent protein 2.3 (VSFP2.3) (19)] exclusively in either cardiomyocytes

Significance

Heart pumping is triggered and coordinated by action potentials (APs) originating in and spreading among electrically excitable heart muscle cells (myocytes) via electrotonic coupling. Cardiac nonmyocytes are thought not to participate in AP conduction in situ, although heterocellular electrotonic coupling is common in cell culture. We used optogenetic tools involving cell-specific expression of a voltage-reporting fluorescent protein to monitor electrical activity in myocytes or nonmyocytes of mouse hearts. We confirm the suitability of this technique for measuring cell type-specific voltage signals and show that, when expressed in nonmyocytes, myocyte AP-like signals can be recorded in cryoinjured scar border tissue. This direct evidence of heterocellular electrotonic coupling in the whole heart necessitates a review of current concepts on cardiac electrical connectivity.

Author contributions: T.A.Q. and P.K. designed research; T.A.Q., P.C., E.A.R.-Z., U.S., T.P., and E.T.O. performed research; T.K. contributed new reagents/analytic tools; T.A.Q., P.C., E.A.R.-Z., and E.T.O. analyzed data; and T.A.Q. and P.K. wrote the paper.

The authors declare no conflict of interest.

This article is a PNAS Direct Submission.

Freely available online through the PNAS open access option.

[1]T.A.Q., P.C., and E.A.R.-Z. contributed equally to this work.

[2]To whom correspondence may be addressed. Email: alex.quinn@dal.ca or peter.kohl@universitaets-herzzentrum.de.

This article contains supporting information online at www.pnas.org/lookup/suppl/doi:10.1073/pnas.1611184114/-/DCSupplemental.

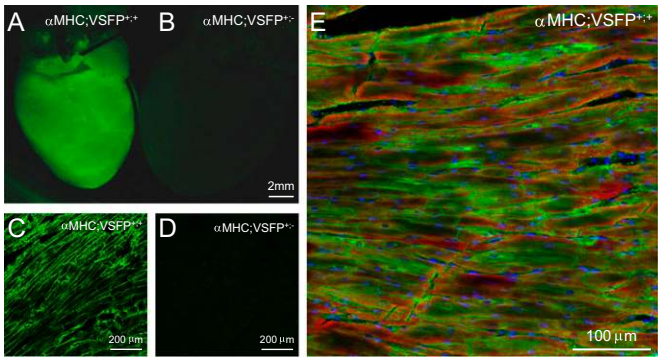

Fig. 1. VSFP2.3 is highly expressed in myocytes of αMHC;VSFP2.3$^{+;+}$ mice. (*A–D*) YFP fluorescence in (*A* and *B*) whole hearts and (*C* and *D*) histological sections of LV tissue immunolabeled with anti-YFP antibody showing (*A*) high and uniform VSFP2.3 expression localized at (*C*) the myocyte sarcolemma in αMHC;VSFP2.3$^{+;+}$ mice, with (*B* and *D*) no discernible expression in αMHC;VSFP2.3$^{+;-}$ mice. (*E*) Representative immunohistochemical staining of VSFP2.3 (anti-YFP antibody; green), cell nuclei (DAPI; blue), and myocytes (antisarcomeric α-actinin antibody; red) in a histological section of LV tissue from an αMHC;VSFP2.3$^{+;+}$ mouse, with extensive colabeling showing high specificity of myocyte targeting.

or nonmyocytes of mice. Cell type-specific expression was achieved using Cre-lox recombination with α-myosin heavy chain [αMHC (20)] targeting VSFP2.3 to cardiomyocytes [αMHC-Cre;double-floxed and inverted reading frame (FLEX)-VSFP2.3 double-transgenic mice] or Wilm's tumor suppressor 1 [WT1 (21)] targeting VSFP2.3 to nonmyocytes (WT1-Cre;FLEX-VSFP2.3 double-transgenic mice).

Results

Myocyte-Specific VSFP2.3 Expression and Voltage Mapping. We first used double-transgenic αMHC;VSFP2.3 mice to assess the suitability of VSFP2.3 with our indicator mouse line for monitoring cardiac electrical activity and to evaluate typical myocyte-generated voltage signal dynamics in our preparation. Presence and spatial distribution of VSFP2.3 expression were established by YFP fluorescence imaging from the whole heart (Fig. 1 *A* and *B*) and anti-YFP antibody staining in histological sections of left ventricular (LV) tissue (Fig. 1 *C* and *D*). In αMHC;VSFP2.3$^{+;+}$ mice, VSFP2.3 is located at the sarcolemma of cardiomyocytes (Fig. 1*C*), whereas controls lacking one transgene (αMHC;VSFP2.3$^{-;+}$ or αMHC;VSFP2.3$^{+;-}$) show no discernible VSFP2.3 expression (e.g., Fig. 1*D*). Targeting efficacy of VSFP2.3 in αMHC;VSFP2.3$^{+;+}$ mice was assessed by immunohistochemical staining of VSFP2.3 (YFP antibody), cell nuclei (DAPI), and myocytes (antisarcomeric α-actinin antibody). Colabeling showed that 98.3 ± 0.5% of myocytes express VSFP2.3 (Fig. 1*E*) (3,170 myocytes, 21 tissue regions, and eight sections from three mice analyzed).

Cardiac electrical activity was studied by epicardial microscopic fluorimetry in excised, excitation–contraction uncoupled (blebbistatin; to exclude motion-related artifacts), Langendorff-perfused hearts from αMHC;VSFP$^{+;+}$ mice. Collection of CFP and YFP fluorescence (300 × 600-μm area) allows measurement of myocyte AP in αMHC;VSFP2.3$^{+;+}$ hearts ($n = 8$). Membrane depolarization decreases CFP and increases YFP fluorescence, enabling signal enhancement by YFP/CFP ratiometry (Fig. 2*A*). To assess VSFP2.3 signal kinetics, hearts were additionally (and cell-indiscriminately) stained by coronary perfusion of a voltage-sensitive fluorescent dye (di-4-ANBDQPQ) (22). As in a previous report (23), VSFP2.3 reliably captures cardiac AP presence. Because of slow voltage-reporting kinetics, the recorded time course of the AP shows an apparently slower AP upstroke and delayed repolarization compared with di-4-ANBDQPQ signals (Fig. 2*B*, Fig. S1, and Movie S1 vs. Movie S2).

Nonetheless, these results confirm the utility of VSFP2.3 for mapping of myocyte-specific electrical activity in the murine whole heart.

Nonmyocyte-Specific VSFP2.3 Expression and Voltage Mapping. To determine whether cardiomyocytes transmit their AP waveforms into nonmyocytes, WT1;VSFP2.3 double-transgenic mice were used. It has been shown previously that scarring potentially enhances heterocellular electrotonic coupling (24, 25) and that WT1 is up-regulated by cardiac injury (26). Therefore, WT1;VSFP2.3$^{+;+}$ and WT1;VSFP2.3$^{+;-}$ mice were subjected to standardized LV epicardial cryoinjury (or sham operation) to focus enhanced expression of VSFP2.3 to nonmyocytes potentially involved in heterocellular electrotonic coupling and studied at 8 wk (±1 d) postsurgery.

Trichrome staining of whole-heart slices shows a compact, nontransmural scar in the cryoinjured LV subepicardium with nearly no surviving myocytes in the bulk scar tissue (Fig. 3*H*). Presence and spatial distribution of VSFP2.3 expression were assessed by anti-YFP antibody staining in histological sections, as above. Fluorescence from interstitial nonmyocytes is increased after cryoinjury in WT1;VSFP2.3$^{+;+}$ mice (Fig. 3*A*) compared to sham-operated control animals (Fig. 3 *C* and *E*). WT1;VSFP2.3$^{-;+}$ and WT1;VSFP2.3$^{+;-}$ mice show no discernible fluorescence with (Fig. 3*B*) or without (Fig. 3*D*) cryoinjury. In cryoinjured WT1;VSFP2.3$^{+;+}$ hearts, VSFP2.3 expression is slightly increased in remote tissue (compared with sham controls); more pronounced elevation is seen in the scar border zone and the central scar (Fig. 3 *A* and *E*) (sham: 69 regions, 15 sections, three mice; remote: 29 regions, 15 sections, three mice; border: 32 regions, 15 sections, three mice; scar: 26 regions, 15 sections, three mice; $P < 0.0001$). In sham hearts, fluorescence is distributed evenly across the ventricular wall (Fig. 3 *F* and *G*) (subepicardium: 47 regions, 14 sections, three mice; midmyocardium: 42 regions, 14 sections, three mice; subendocardium: 43 regions, 14 sections, three mice; $P > 0.05$).

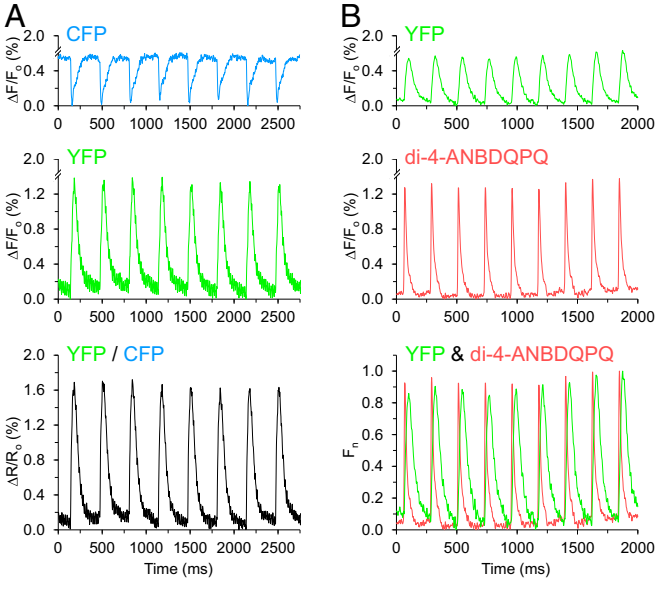

Fig. 2. VSFP2.3 reports electrical activity of myocytes in αMHC;VSFP2.3$^{+;+}$ hearts. (*A*) CFP (blue) and YFP (green) fluorescence (F; expressed as percentage change $\Delta F/F_o$) simultaneously collected from the LV epicardium of an αMHC;VSFP2.3$^{+;+}$ mouse heart showing electrical activity of myocytes, with signal enhancement by YFP/CFP ratiometry (black; expressed as percentage $\Delta R/R_o$). (*B*) Simultaneously collected YFP (green) (Fig. S1*A* and Movie S1) and voltage-sensitive fluorescent dye di-4-ANBDQPQ (red) (Fig. S1*B* and Movie S2) fluorescence in αMHC;VSFP2.3$^{+;+}$ mouse heart and their normalized comparison (F_n), illustrating the known slower de- and repolarization kinetics of VSFP2.3 compared to di-4-ANBDQPQ signals but otherwise, good AP detection fidelity.

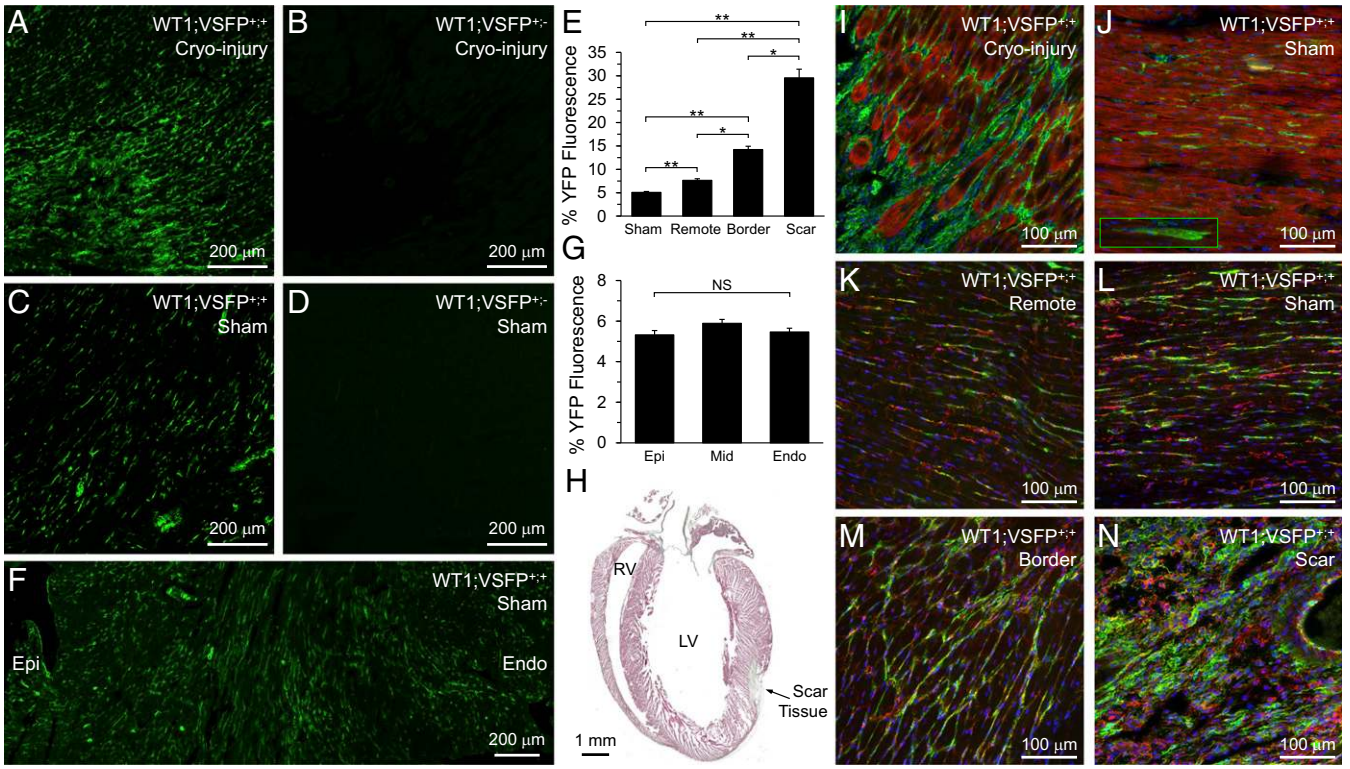

Fig. 3. VSFP2.3 is highly expressed in nonmyocytes but not myocytes of WT1;VSFP2.3$^{+;+}$ mice. (*A–G*) YFP fluorescence in histological sections of LV tissue showing increased VSFP2.3 expression as detected by anti-YFP antibody in interstitial nonmyocytes of (*A*) cryoinjured vs. (*C*) sham-operated WT1;VSFP2.3$^{+;+}$ mice, lack of expression in WT1;VSFP2.3$^{+;-}$ mice (*B*) with and (*D*) without cryoinjury, (*E*) increase in expression from remote tissue to the scar border and into the scar in injured hearts, and (*F* and *G*) evenly distributed expression across the ventricular wall in sham hearts. Endo, subendocardium; Epi, subepicardium; Mid, mid-myocardium; NS, not significant. *$P < 0.05$; **$P < 0.001$. (*H*) Trichrome-stained longitudinal section of a cryoinjured heart showing the extent of scar tissue (collagen is stained bluish green, and myocytes are stained pink). RV, right ventricle. (*I–N*) Immunohistochemical staining of VSFP2.3 (green), cell nuclei (blue), and (*I* and *J*) myocytes (red) or (*K–N*) nonmyocytes (red) in histological sections of LV tissue from WT1;VSFP2.3$^{+;+}$ mice, with colabeling showing lack of VSFP2.3 in myocytes of (*I*) cryoinjured and (*J*) sham-operated animals (a rare example of a VSFP2.3-expressing myocyte is shown in *Inset*) but high nonmyocyte-specific expression in the remote tissue of (*K*) cryoinjured and (*L*) sham hearts, which increases (*M*) in the scar border and (*N*) into the scar. Data are presented as mean ± SEM; $n \geq 26$ per group.

To determine cell type specificity of VSFP2.3 expression, immunohistochemical analysis of slices from cryoinjured, sham-operated, and intervention-free WT1;VSFP2.3$^{+;+}$ mice was performed as above, with the addition of nonmyocyte staining (antivimentin antibody). Colabeling of YFP and sarcomeric α-actinin showed that virtually no myocytes express VSFP2.3 in cryoinjured WT1;VSFP2.3$^{+;+}$ hearts (Fig. 3*I*), in whom the percentage of YFP/α-actinin–colabeled cells is negligible [remote myocardium: 0.33 ± 0.08%; 5,359 myocytes, 24 regions, 12 sections, three mice; scar border zone: 0.06 ± 0.003%; 4,347 myocytes, 22 regions, 12 sections, three mice; central scar tissue: 0%; 87 myocytes (very few surviving myocytes were found), 20 regions, 10 sections, three mice]. Sham-operated WT1;VSFP2.3$^{+;+}$ hearts also display negligible VSFP2.3 expression in cardiomyocytes (Fig. 3*J*) (0.18 ± 0.06%; 5,189 myocytes, 23 regions, 12 sections, three mice) as do intervention-free hearts (0.22 ± 0.06%; 889 myocytes, 15 regions, 5 sections, two mice).

Measurement of YFP and vimentin colabeling, however, showed VSFP2.3 expression in a large percentage of nonmyocytes in the remote tissue of cryoinjured hearts (Fig. 3*K*) (40.8 ± 1.5%; 10,098 cells, 28 regions, 15 sections, three mice) as well as in sham-operated (Fig. 3*L*) (41.6 ± 1.7%; 10,538 cells, 29 regions, 15 sections, three mice) and intervention-free hearts (41.0 ± 1.0%; 2,216 cells, 20 regions, 6 sections, three mice). The similar fraction of VSFP2.3-expressing nonmyocytes but higher absolute VSFP2.3 fluorescence in remote vs. sham tissue (Fig. 3*E*) suggest an increase in number or size of nonmyocytes in the remote regions of cryoinjured hearts. Postcryoinjury, the fraction of vimentin-positive cells that express VSFP2.3 is increased in the scar border zone (Fig. 3*M*) (61.2 ± 1.3%; 9,987 cells, 26 regions, 15 sections, three mice) and the central scar (Fig. 3*N*) (71.1 ± 1.6%; 11,850 cells, 25 regions, 15 sections, three mice).

Epicardial fluorescence was assessed microscopically (600 × 600-μm area) by sequential measurements across the LV surface of Langendorff-perfused hearts from cryoinjured, sham-operated, and intervention-free WT1;VSFP2.3$^{+;+}$ mice. No dynamic changes in VSFP2.3 fluorescence were seen in remote tissue or the central scar of cryoinjured hearts ($n = 4$) (Fig. 4) or in sham-operated ($n = 4$) and intervention free ($n = 4$) controls, indicating either a lack of significant transmembrane potential changes in cardiac nonmyocytes or, if present, inadequate signal strength to observe them. In contrast, clear VSFP2.3 signal changes resembling myocardial AP waveforms in shape and time course were recorded at the border between cryoinjured and healthy tissue (in three of four cryoinjured hearts) (Fig. 4, Fig. S2, and Movie S3) and, with lower amplitude, in adjacent tissue (Fig. 4). This observation suggests that, in the border zone, nonmyocytes can be electrotonically driven by electrically coupled cardiomyocytes to passively display AP-like potential oscillations.

Overall, our results show that WT1-driven expression of VSFP2.3 occurs in a significant fraction of cardiac nonmyocytes (but not of myocytes) and that this fraction is up-regulated after cryoinjury. In scar border tissue, VSFP2.3 reports the electrical signature activity generated by excitable heart muscle cells, although the reporter protein is expressed near-exclusively in electrically nonexcitable nonmyocytes (i.e., in ∼60% of vimentin-positive nonmyocytes vs. ∼0.06% of myocytes—four orders of magnitude separation). This

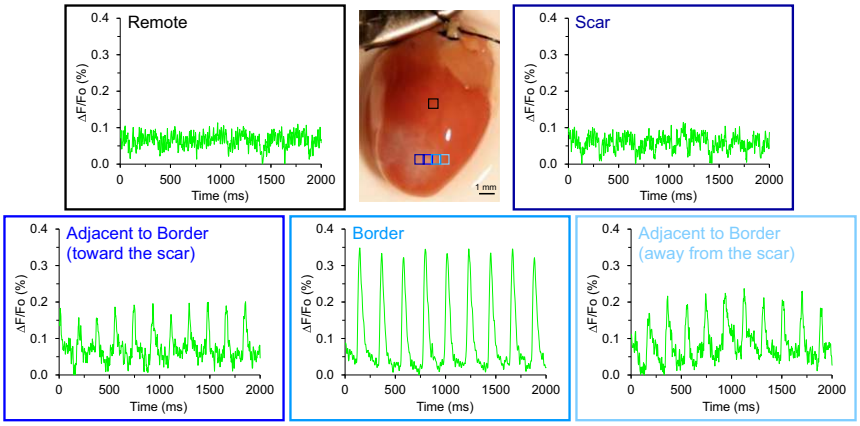

Fig. 4. VSFP2.3 reports electrical activity of nonmyocytes at the scar border in WT1;VSFP2.3$^{+/+}$ hearts. YFP fluorescence (F; expressed as percentage change $\Delta F/F_o$) collected from remote, central scar, scar border, and adjacent tissue (both toward and away from the scar center) in a WT1;VSFP2.3$^{+/+}$ mouse heart showing AP-like electrical activity in nonmyocytes at the scar border (indicating electrotonic signal transmission from myocytes to nonmyocytes) (Fig. S2 and Movie S3) and with lower amplitude in adjacent tissue (suggesting reduced passively conducted signal amplitude toward the scar center and reduced heterocellular electrotonic coupling away from the scar). No rhythmic polarizations were seen in central scar or remote tissue. [The number of fluorescence oscillations in border vs. adjacent tissue differed due to nonsimultaneous recordings.]

effect can be explained by electrotonic coupling of myocytes and nonmyocytes in the scar border zone and propagation of AP-shaped polarizations from the former to the latter. This finding provides direct evidence for functional electrical signal transmission from myocytes to nonmyocytes in whole heart.

Structural Connectivity of Myocytes and Nonmyocytes. Plausible structural substrates for heterocellular electrotonic coupling include previously identified connexin-based junctions between cardiac myocytes and nonmyocytes in situ (5) but potentially also tunneling nanotubes (27). These direct membrane connections have been shown to support heterocellular communication (28), including electrotonic coupling (29), in vitro. To investigate 3D nanoscale interrelations of myocytes and nonmyocytes at the scar border of cryoinjured hearts, tissue samples were imaged by electron tomography (ET) with an isotropic voxel size of 1.02–2.55 nm. ET revealed a high prevalence of membrane protrusions originating predominantly from nonmyocytes and extending toward/connecting with myocytes (Fig. 5). These protrusions were observed in all of the ET reconstructions of scar border myocyte–nonmyocyte contact regions analyzed (seven cell pairs, 11 samples; total number of voxels analyzed $>35 \times 10^9$), with one to seven protrusions per nonmyocyte-containing tomogram (275 nm across the z axis). Nonmyocyte protrusions had a mean length of 293.5 ± 44.5 nm (ranging from 39.7 nm to 1.381 μm) and a mean diameter of 22.3 ± 3.5 nm (ranging from 3.8 to 54.8 nm; 42 protrusions analyzed). No spatial preference for the point of contact along the sarcomeric structure of myocytes (relative to Z or M lines) was identifiable. Occasionally, nonmyocyte protrusions were in contact with smaller and shorter sarcolemmal projections that originate from myocytes and extend past the basement membrane (Fig. 5D and Movie S4).

Discussion

Using an optogenetic approach for cell type-specific targeting of a genetically encoded voltage indicator, we observed myocyte AP-like changes in membrane voltage in nonexcitable cells at the border of cardiac scar tissue. This finding provides functional evidence of heterocellular electrotonic coupling in the heart and calls for a revised conceptual approach to cardiac electrophysiology that acknowledges the plausibility of nonmyocyte contributions to (passive) propagation of cardiac electrical activity.

The possibility of electrotonic coupling between myocytes and nonexcitable cells and the functional significance of resulting electrical interactions for cardiac electrophysiology were first proposed some two decades ago (18) but never functionally substantiated in native myocardium [beyond circumstantial evidence from dye transfer experiments in one rabbit atrial tissue

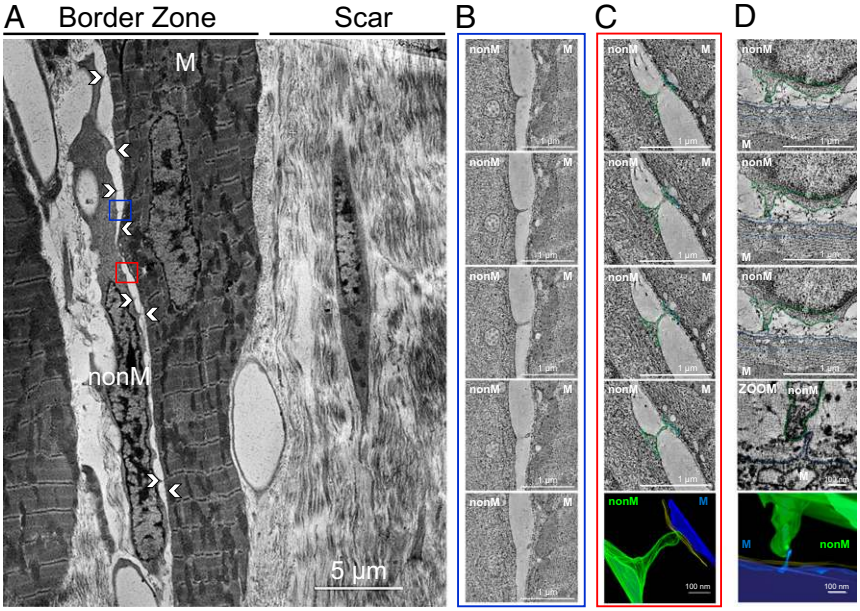

Fig. 5. Tunneling nanotubes connecting nonmyocytes to myocytes at the scar border. (*A*) Thick section (275-nm) transmission electron micrograph showing extensive finger-like membrane protrusions (examples indicated by white arrowheads) extending from a nonmyocyte to a myocyte in the scar border zone. (*B* and *C*) Serial ET slices (separated by 20 nm in the z axis) reconstructed in the plane of membrane protrusions indicated by the (*B*) blue and (*C*) red boxes in *A*, including (*C*, row 5) a segmentation and 3D rendering representing nonmyocyte sarcolemma (green), myocyte surface sarcolemma (blue), and myocyte basement membrane (yellow). In addition to nonmyocyte-derived nanotubes that either (*B*) extend toward the myocyte basement membrane or (*C*) penetrate that to contact the myocyte sarcolemma, (*D*) occasionally both cell types possess sarcolemmal membrane extensions toward one other (Movie S4). M, myocyte; nonM, nonmyocyte.

study (6) and more recent evidence from a connexin 43 knockout mouse model (7)]. There are several important clinical implications of electrical connectivity between myocytes and nonmyocytes. Electrotonic coupling may interfere with the success of therapeutic interventions, such as atrial ablation, by causing scars to become "electrically transparent" with time (perhaps, in particular, between ablation points, where scars are most narrow). Such "disappearance" of intraprocedurally confirmed lesions seems to occur in a majority of atrial ablation patients (8). Although atrial ablation lines, placed to electrically separate adjacent muscle regions, may perhaps be discontinuous to begin with (even if, intraprocedurally, block is achieved), de novo formation of electrical conduction across continuous and fully transmural scars after surgery has also been reported (9, 10). The simplest explanation of these phenomena is passive AP conduction via nonmyocyte bridges electrically connecting (and activating) otherwise isolated groups of cardiac myocytes, as seen in cell culture (14, 15). Heterocellular electrotonic coupling that links groups of surviving myocytes could also explain conduction of electrical excitation into postinfarct (11) and cryoinjury scar tissue (7). It would also appear to be a key determinant of the success of engineered heterocellular tissue grafts, implanted to patch up cardiac conduction [e.g., to fix atrioventricular block (12, 13)]. Additionally, effects of nonmyocytes on myocyte electrophysiology and AP propagation in fibrotic tissue may be arrhythmogenic by contributing to reentrant pathways and by altering excitability, repolarization, and conduction in heart muscle (30).

It may be argued that the voltage signals measured at the scar border in WT1;VSFP2.3$^{+;+}$ mice could have originated from the minute number of individual myocytes expressing the protein rather than nonmyocytes. The spurious expression of VSFP2.3 in myocytes (~0.06% in the border zone) may potentially be explained by WT1-expressing cell progeny among myocytes (31, 32) or VSFP2.3 trafficking via the observed tunneling nanotubes [if they form continuous plasma membrane conduits as reported in some cell culture models (27)]. However, if VSFP2.3 signals in WT1;VSFP2.3$^{+;+}$ mice had originated from myocytes, then one would expect to also observe them in other ventricular tissue regions where the fraction of VSFP2.3 expressing myocytes, if anything, is higher. These areas include remote regions of cryoinjured hearts (~0.33%), sham-operated hearts (~0.18%), and intervention-free hearts (~0.22%). However, in no single case were AP-like voltage swings observed in any of these areas ($n = 0/12$ hearts), whereas in scar border tissue AP waveforms were seen in $n = 3/4$ hearts.

Although it would have been desirable to map the entire LV surface in one view, surface mapping was prevented by spatially confined localization (border zone) and limited signal strength in WT1;VSFP2.3$^{+;+}$ hearts, necessitating sequential microscopic measurements across the LV surface. The microscopic nature (600 × 600-μm area) of measurements has the advantage of further reducing the probability of contributions from VSFP2.3-expressing myocytes to observed voltage signals in WT1;VSFP2.3$^{+;+}$ hearts. Compared to the relatively uniform excitation patterns seen in αMHC;VSFP2.3$^{+;+}$ mice (Fig. S1*A* and Movie S1), in WT1;VSFP2.3$^{+;+}$ mice we observed patchy, locally heterogeneous excitation, notably with no discernible lateral translocation of sources that would have been indicative of motion artifacts (Fig. S2 and Movie S3). Adjacent tissue regions showed similar signals, although of lower amplitude, suggesting a reduction in passively conducted signal amplitude in the direction of the scar center and reduced heterocellular electrotonic coupling in surviving myocardium with increasing distance away from the scar (Fig. 4).

Although the use of blebbistatin eliminated discernable contractile activity, microscopic motion may be present, including the possibility of motion in the surface-normal direction. A lack of motion artifact in the AP-like signals seen at the scar border in WT1;VSFP2.3$^{+;+}$ hearts is supported by the fact that the CFP signal recorded at the same location did not show an increase in fluorescence similar to that of YFP that would indicate a contribution of motion to the recorded signals (Fig. S3) (the fact that we found no consistent decrease in CFP fluorescence during AP activity is caused by the weakness of the signal).

Thus, it seems that nonmyocytes can indeed passively mimic the electrical activity of myocytes in the heart, at least at the border of scar tissue, where there is a large myocyte–nonmyocyte interface offering a beneficial source–sink relation for myocytes to AP-clamp nonmyocytes. This finding corroborates the principal possibility of heterocellular electrotonic coupling of excitable and nonexcitable cells in situ. The lack of measured AP-like activity in healthy tissue (i.e., in sham WT1;VSFP2.3$^{+;+}$ mice or remote tissue of cryoinjured animals) may indicate an absence (or smaller degree) of heterocellular electrotonic coupling in these regions; alternatively, it may be accounted for by insufficient signal strength because of the lower VSFP2.3 expression per volume of intact (myocyte-dominated) tissue. One potential explanation for a difference in heterocellular electrotonic coupling is that, at the scar border, such coupling would involve "activated" nonmyocytes [e.g., myofibroblasts (30)]. In contrast, the lack of measured electrical activity in the central scar (where VSFP2.3 expression was high) may be explained by the distance from AP-generating cells at the scar border (10^{-3}-m domain), whereas nonmyocyte-mediated AP propagation terminates in the 10^{-4}-m region in cell culture (14). Longer-distance AP propagation may be possible if passive conduction via nonmyocytes reaches AP-generating cells (acting as "repeater stations") in tissue containing a mix of both cell types, as documented for engineered tissue strands (12, 13). Postinfarction scars, for example, tend to contain interspersed groups of surviving myocytes; this finding is less common in postablation scars (including our cryoinjured hearts).

From our results, a range of exciting research targets emerges, including the extent, regulation, and roles of heterocellular electrical connectivity in healthy and diseased cardiac tissue and the contribution (and possible cooperativity) of underlying structural substrates, such as connexins (6, 7) and tunneling nanotubes (27–29).

Electronic coupling between excitable and nonexcitable cells would also be important for more general physiology (for instance, related to communication between neurons and neuroglia) (33). Heterocellular electrical coupling in the CNS may be a crucial player in the development of epilepsy (34) and ischemic brain damage (35). Additional insight into underlying mechanisms will benefit from optogenetic targeting of reporter proteins to various cell subpopulations in excitable organs.

For the heart in particular, excitable–nonexcitable cell cross-talk has potentially far-reaching conceptual, physiological, pathological, and therapeutic implications (36), because—in the long run—it may allow one to steer atrial scars to remain electrically insulating postablation (e.g., by preventing heterocellular coupling) or in contrast, to preserve uniform ventricular conduction across small postinfarct scars (by locally increasing nonmyocyte-mediated AP conduction in the heart).

Methods

Experiments were conducted under ethical approval in accordance with the United Kingdom Animals (Scientific Procedures) Act of 1986 and the Position of the American Heart Association on Research Animal Use. Methods are summarized here, and details are in *SI Methods*.

Animal Model, Surgical Procedures, and Isolated Heart Preparation. Cell type-specific expression of VSFP2.3 (19) was achieved by Cre-lox recombination using FLEX, which allowed for the required levels of cell specificity by preventing off-target expression, with αMHC for targeting expression to cardiomyocytes (20) or WT1 for targeting expression to nonmyocytes (21). Adult WT1;VSFP2.3$^{+;+}$ and WT1;VSFP2.3$^{+;-}$ mice were subjected to sham operation ($n = 4$ WT1;VSFP2.3$^{+;+}$ mice, $n = 2$ WT1;VSFP2.3$^{+;-}$ mice) or standardized LV epicardial cryoinjury ($n = 4$ WT1;VSFP2.3$^{+;+}$ mice, $n = 3$ WT1;VSFP2.3$^{+;-}$ mice) to generate a nontransmural

subepicardial scarred region. Isolated hearts were Langendorff-perfused with 37 °C Tyrode solution in a temperature-controlled chamber.

Measurement of Electrical Activity. Subepicardial electrical activity was collected sequentially across the surface of the LV by microscopic fluorimetry. Hearts were excitation–contraction uncoupled with 10 μM (±)-blebbistatin (Abcam). Eight αMHC;VSFP2.3$^{+/+}$ hearts (nonsurgery controls) were additionally stained with a voltage-sensitive fluorescent dye [di-4-ANBDQPQ; University of Connecticut Health Center (22)]. For simultaneous dual-wavelength emission imaging, fluorescence at each wavelength was collected at 511 frames per second from a 300 × 600-μm area onto one-half of a 128 × 128-pixel electron multiplying charge-coupled device camera (Cascade:128+; Photometrics). For collection of a single wavelength, fluorescence was collected from a 600 × 600-μm area onto the entire camera sensor. Signals were analyzed with custom routines in MATLAB (R2014a; MathWorks).

Histology. Cryosections were imaged with a confocal laser-scanning microscope (LSM 510 Meta; Carl Zeiss). VSFP2.3 was labeled using rabbit anti-YFP antibody (ab290; Abcam) and secondary donkey anti-rabbit Alexa488 (Life Technologies). Myocytes were labeled with a mouse antisarcomeric α-actinin antibody (ab9465; Abcam) and Alexa568 (Z-25006; Life Technologies). Nonmyocytes were labeled using a guinea pig antivimentin antibody (GP53; Progen Biotechnik) and a donkey anti-guinea pig CY3 (Jackson ImmunoResearch Laboratories). Total VSFP2.3 expression was quantified by YFP immunolabeling (reported as percentage fluorescence relative to tissue area) using ImageJ (imagej.nih.gov/ij/), whereas cell specificity and efficiency of expression were measured by counting cells costained for YFP and sarcomeric α-actinin or vimentin (reported as percentage of total α-actinin–positive myocytes or vimentin-positive nonmyocytes, respectively).

3D EM Tomography. Preparations were imaged at the Boulder Laboratory for 3D Electron Microscopy of Cells (University of Colorado) using an intermediate voltage electron microscope (Tecnai TF30; FEI) with an isotropic voxel size of 1.02–2.55 nm. Dual-axis tilt series images were back-projected to generate two single full-thickness reconstructed volumes (tomograms) using IMOD (bio3d.colorado.edu/imod/), which were combined to generate a single high-resolution 3D reconstruction (37).

Statistical Analysis. Values were expressed as mean ± SEM. Analyses were performed using Graphpad Prism, with a significance of $P < 0.05$. Differences across groups were evaluated by ANOVA followed by posthoc Dunn's test comparisons.

ACKNOWLEDGMENTS. We thank Jakki A. Kelly-Barrett for assistance in performing cryoinjury surgeries, Andreas Hoenger and the Boulder Laboratory for 3D Electron Microscopy of Cells (funded by NIH Grant P41-GM103431) for support with 3D ET, Michael D. Schneider for providing αMHC promotor Cre mice, Leslie M. Loew for access to di-4-ANBDQPQ, the Boehringer Ingelheim Fonds for early support of the ideas underlying this study (postdoctoral fellowship to P.K.), and the Fox Chase Cancer Center for providing WT1 promotor Cre mice. T.A.Q. is funded by Canadian Institutes of Health Research Grant MOP-142424, Natural Sciences and Engineering Research Council Grant RGPIN-2016-04879, and Nova Scotia Health Research Foundation Grant MED-EST-2014-9582. T.A.Q. is a National New Investigator of the Heart and Stroke Foundation, E.A.R-Z. is an Immediate Postdoctoral Fellow, and P.K. a Senior Fellow, of the British Heart Foundation. Generation of VSFP2.3 mice was supported by an RIKEN Intramural Grant (to T.K.). This work was supported by European Research Council Advanced Grant CardioNECT (to P.K.) and the Magdi Yacoub Institute.

1. Camelliti P, Borg TK, Kohl P (2005) Structural and functional characterisation of cardiac fibroblasts. *Cardiovasc Res* 65(1):40–51.
2. Adler CP, Ringlage WP, Böhm N (1981) [DNA content and cell number in heart and liver of children. Comparable biochemical, cytophotometric and histological investigations (author's transl)]. *Pathol Res Pract* 172(1-2):25–41.
3. Kohl P, Gourdie RG (2014) Fibroblast-myocyte electrotonic coupling: Does it occur in native cardiac tissue? *J Mol Cell Cardiol* 70:37–46.
4. Mahoney VM, Mezzano V, Morley GE (2016) A review of the literature on cardiac electrical activity between fibroblasts and myocytes. *Prog Biophys Mol Biol* 120(1-3): 128–133.
5. Kohl P, Camelliti P (2012) Fibroblast-myocyte connections in the heart. *Heart Rhythm* 9(3):461–464.
6. Camelliti P, Green CR, LeGrice I, Kohl P (2004) Fibroblast network in rabbit sinoatrial node: Structural and functional identification of homogeneous and heterogeneous cell coupling. *Circ Res* 94(6):828–835.
7. Mahoney VM, et al. (2016) Connexin43 contributes to electrotonic conduction across scar tissue in the intact heart. *Sci Rep* 6:26744.
8. Pratola C, Baldo E, Notarstefano P, Toselli T, Ferrari R (2008) Radiofrequency ablation of atrial fibrillation: Is the persistence of all intraprocedural targets necessary for long-term maintenance of sinus rhythm? *Circulation* 117(2):136–143.
9. Hager A, et al. (2005) Congenital and surgically acquired Wolff-Parkinson-White syndrome in patients with tricuspid atresia. *J Thorac Cardiovasc Surg* 130(1):48–53.
10. Lefroy DC, et al. (1998) Recipient-to-donor atrioatrial conduction after orthotopic heart transplantation: Surface electrocardiographic features and estimated prevalence. *Am J Cardiol* 82(4):444–450.
11. Walker NL, Burton FL, Kettlewell S, Smith GL, Cobbe SM (2007) Mapping of epicardial activation in a rabbit model of chronic myocardial infarction. *J Cardiovasc Electrophysiol* 18(8):862–868.
12. Choi YH, et al. (2006) Cardiac conduction through engineered tissue. *Am J Pathol* 169(1):72–85.
13. Cingolani E, et al. (2014) Engineered electrical conduction tract restores conduction in complete heart block: From in vitro to in vivo proof of concept. *J Am Coll Cardiol* 64(24):2575–2585.
14. Gaudesius G, Miragoli M, Thomas SP, Rohr S (2003) Coupling of cardiac electrical activity over extended distances by fibroblasts of cardiac origin. *Circ Res* 93(5): 421–428.
15. Goshima K, Tonomura Y (1969) Synchronized beating of embryonic mouse myocardial cells mediated by FL cells in monolayer culture. *Exp Cell Res* 56(2):387–392.
16. Nussinovitch U, Shinnawi R, Gepstein L (2014) Modulation of cardiac tissue electrophysiological properties with light-sensitive proteins. *Cardiovasc Res* 102(1):176–187.
17. Rook MB, et al. (1992) Differences in gap junction channels between cardiac myocytes, fibroblasts, and heterologous pairs. *Am J Physiol* 263(5 Pt 1):C959–C977.
18. Kohl P, Kamkin AG, Kiseleva IS, Noble D (1994) Mechanosensitive fibroblasts in the sino-atrial node region of rat heart: Interaction with cardiomyocytes and possible role. *Exp Physiol* 79(6):943–956.
19. Lundby A, Mutoh H, Dimitrov D, Akemann W, Knöpfel T (2008) Engineering of a genetically encodable fluorescent voltage sensor exploiting fast Ci-VSP voltage-sensing movements. *PLoS One* 3(6):e2514.
20. Agah R, et al. (1997) Gene recombination in postmitotic cells. Targeted expression of Cre recombinase provokes cardiac-restricted, site-specific rearrangement in adult ventricular muscle in vivo. *J Clin Invest* 100(1):169–179.
21. Wessels A, et al. (2012) Epicardially derived fibroblasts preferentially contribute to the parietal leaflets of the atrioventricular valves in the murine heart. *Dev Biol* 366(2): 111–124.
22. Matiukas A, et al. (2007) Near-infrared voltage-sensitive fluorescent dyes optimized for optical mapping in blood-perfused myocardium. *Heart Rhythm* 4(11):1441–1451.
23. Chang Liao ML, et al. (2015) Sensing cardiac electrical activity with a cardiac myocyte–targeted optogenetic voltage indicator. *Circ Res* 117(5):401–412.
24. Vasquez C, et al. (2010) Enhanced fibroblast-myocyte interactions in response to cardiac injury. *Circ Res* 107(8):1011–1020.
25. Zhang Y, Kanter EM, Yamada KA (2010) Remodeling of cardiac fibroblasts following myocardial infarction results in increased gap junction intercellular communication. *Cardiovasc Pathol* 19(6):e233–e240.
26. Duim SN, Kurakula K, Goumans MJ, Kruithof BP (2015) Cardiac endothelial cells express Wilms' tumor-1: Wt1 expression in the developing, adult and infarcted heart. *J Mol Cell Cardiol* 81:127–135.
27. Davis DM, Sowinski S (2008) Membrane nanotubes: Dynamic long-distance connections between animal cells. *Nat Rev Mol Cell Biol* 9(6):431–436.
28. He K, et al. (2011) Long-distance intercellular connectivity between cardiomyocytes and cardiofibroblasts mediated by membrane nanotubes. *Cardiovasc Res* 92(1):39–47.
29. Wang X, Veruki ML, Bukoreshtliev NV, Hartveit E, Gerdes HH (2010) Animal cells connected by nanotubes can be electrically coupled through interposed gap-junction channels. *Proc Natl Acad Sci USA* 107(40):17194–17199.
30. Rohr S (2012) Arrhythmogenic implications of fibroblast-myocyte interactions. *Circ Arrhythm Electrophysiol* 5(2):442–452.
31. Zhou B, et al. (2008) Epicardial progenitors contribute to the cardiomyocyte lineage in the developing heart. *Nature* 454(7200):109–113.
32. Smart N, et al. (2011) De novo cardiomyocytes from within the activated adult heart after injury. *Nature* 474(7353):640–644.
33. Giaume C, Naus CC (2013) Connexins, gap junctions, and glia. *WIREs Membr Transp Signal* 2:133–142.
34. Carlen PL (2012) Curious and contradictory roles of glial connexins and pannexins in epilepsy. *Brain Res* 1487:54–60.
35. Beppu K, et al. (2014) Optogenetic countering of glial acidosis suppresses glial glutamate release and ischemic brain damage. *Neuron* 81(2):314–320.
36. Gourdie RG, Dimmeler S, Kohl P (2016) Novel therapeutic strategies targeting fibroblasts and fibrosis in heart disease. *Nat Rev Drug Discov* 15(9):620–638.
37. Mastronarde DN (1997) Dual-axis tomography: An approach with alignment methods that preserve resolution. *J Struct Biol* 120(3):343–352.
38. Quinn TA, et al. (2011) Minimum Information about a Cardiac Electrophysiology Experiment (MICEE): Standardised reporting for model reproducibility, interoperability, and data sharing. *Prog Biophys Mol Biol* 107(1):4–10.
39. Lee P, et al. (2011) Single-sensor system for spatially resolved, continuous, and multiparametric optical mapping of cardiac tissue. *Heart Rhythm* 8(9):1482–1491.
40. Burton RA, et al. (2006) Three-dimensional models of individual cardiac histoanatomy: Tools and challenges. *Ann N Y Acad Sci* 1080:301–319.